SAND REPORT

Assessing Mesoscale Material Response Under Shock & Isentropic Compression Via High-Resolution Line-Imaging VISAR

(Final report for LDRD Project 39669)

Michael D. Furnish, Wayne M. Trott, Joshua Mason, Jason Podsednik, William D. Reinhart and Clint A. Hall.

Sandia National Laboratories

Assessing Mesoscale Material Response Under Shock & Isentropic Compression Via High-Resolution Line-Imaging VISAR

Michael D. Furnish, Jason Podsednik and William D. Reinhart
Solid Dynamics and Energetic Materials Department

Wayne M. Trott
Thermal Fluid and Aero Experimental Sciences Department

Joshua Mason and Clint A. Hall
Shock and Z-Pinch Physics Department 1646

Sandia National Laboratories
P.O. Box 5800
Albuquerque NM 87185-1168

Abstract

Of special promise for providing dynamic mesoscale response data is the line-imaging VISAR, an instrument for providing spatially resolved velocity histories in dynamic experiments. We have prepared two line-imaging VISAR systems capable of spatial resolution in the 10 – 20 micron range, at the Z and STAR facilities. We have applied this instrument to selected experiments on a compressed gas gun, chosen to provide initial data for several problems of interest, including: (1) pore-collapse in copper (two variations: 70 micron diameter hole in single-crystal copper) and (2) response of a welded joint in dissimilar materials (Ta, Nb) to ramp loading relative to that of a compression joint. The instrument is capable of resolving details such as the volume and collapse history of a collapsing isolated pore.

Acknowledgments

We gratefully acknowledge the assistance of Heidi Anderson, who patiently assembled most of the projectiles and targets used here. Jaime Castañeda was indispensable in the fielding of the line-imaging VISAR. Randy Hickman was indispensable for the efforts at Z. As well, we gratefully acknowledge the contribution of the single-crystal copper samples by Vitali Nesterenko (UCSD); the use of samples from the same boule as an earlier set of experiments enhances the value of the present experiments.

Table of Contents

Figures

Assessing Mesoscale Material Response Under Shock & Isentropic Compression Via High-Resolution Line-Imaging VISAR

1.0 Introduction and Motivation

1.1 Introduction: Over the past decade, the forefront of high strain-rate dynamics has shifted from continuum studies to what have been termed mesoscale studies. These studies have sought an improved understanding of the effects of grain boundaries, voids, single dislocations, grain interactions and similar phenomena on loading dynamics (e.g. wave speeds, dispersion, attenuation, detonation onset for energetic materials). Together with this shift of focus has come an increased demand for high spatial-resolution shock diagnostics.

The line-imaging velocity interferometer [Trott, 2000; Hemsing, 1992] is an especially promising recent development. It combines high temporal bandwidth (sub-ns resolution under optimal conditions) with the potential for spatial resolution limited principally by the resolution with which an optical relay can image a sample onto the aperture of a streak camera. In this instrument, a coherently illuminated line on a sample is imaged through a velocity interferometer (VISAR) and onto a streak camera. On the streaked image, motion of the target is indicated by the passage of fringes along lines of constant position (Fig. 1.1).

1.2 Motivation: As an example of the utility of this instrument, consider a macroscale example of line VISAR data. The spallation properties of tantalum have been of interest for several years [Chhabildas et al, 2002]. Spall occurs when a material is dynamically placed in tension sufficient to pull it apart. Fig. 1.2 shows line VISAR data for spall of tantalum with two different grain structures. The experiments utilized a thin flyer plate impacting a thick sample, with VISAR monitoring the free surface of the sample. Colliding release waves from the free surfaces of the flyer plate and the target plate pull the sample into tension and spall it. A reshock wave from the spall surface then travels to the free surface of the target. However, preparation of the tantalum sample has a marked effect on spall properties (tension amplitude required, spatial variations, viscosity). These differences are apparent in Fig. 1.2. The plate stock spalls with greater spatial uniformity and in a sharper plane than does the bar stock, as well as showing a higher spall strength.

Another mesoscale phenomenon is that of the effect of crystallite sizes on phase transition properties. During the setup of the line VISAR instrumentation described herein, we conducted a multipoint VISAR experiment using the Z facility as an ICE driver. On a single panel we placed a C-cut sample of single-crystal calcite ($CaCO_3$)
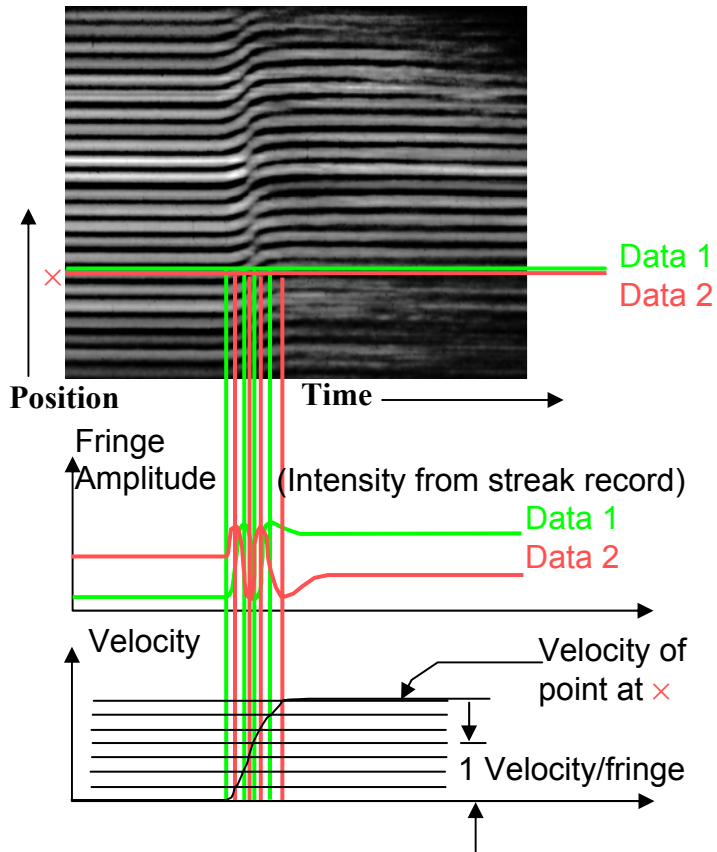
Figure 1.1. Illustration of line ORVIS (VISAR) data. The vertical motion of fringes corresponds to velocity changes at the position corresponding to the lineout. This image corresponds to Data1; other variations use 4 streak records to give full-quadrature records.

and a sample of lithographic limestone (50 micron grains). Each sample was 1 mm thick and 6 mm diameter. The lithographic limestone porosity was approx. 4%. Both were essentially pure calcium carbonate materials. Lithium fluoride windows were attached to both samples and to a section of the copper panel between the samples, as shown in Fig. 1.3. The velocity histories measured by VISAR (Fig. 1.3) show clearly that the individual $CaCO_3$ phase transitions [Ivanov and Deutsch, 2002] so visible in the single-crystal material are not discrete in the lithographic limestone, with its small crystal size.

1.3 Basic issues for High-Resolution Line-Imaging VISAR (ORVIS): Producing a high-resolution line-imaging VISAR requires overcoming certain practical difficulties. In any setting (lab bench, gas gun or pulsed-power facility), an optical relay must be designed which meets magnification and resolution criteria. For 5 – 10 μm resolution, magnification of 17:1 is needed. Gas gun and pulsed power facility layouts impose three additional issues. First, the relay must be at least 12 m long to pass the light from the target to the interferometer in a control room or screen box.
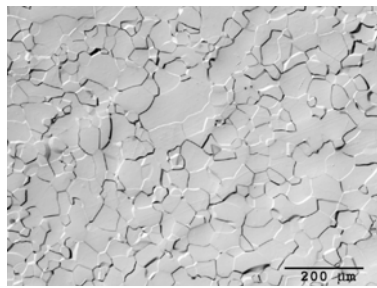
Plate Stock (LANL)
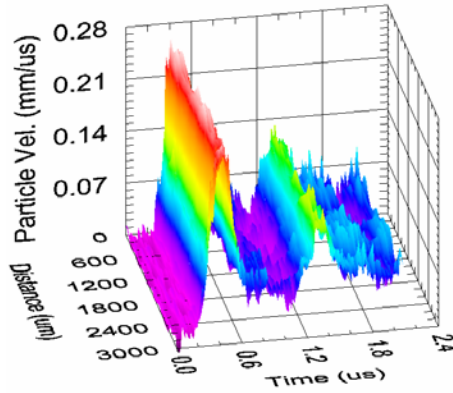
Bar Stock
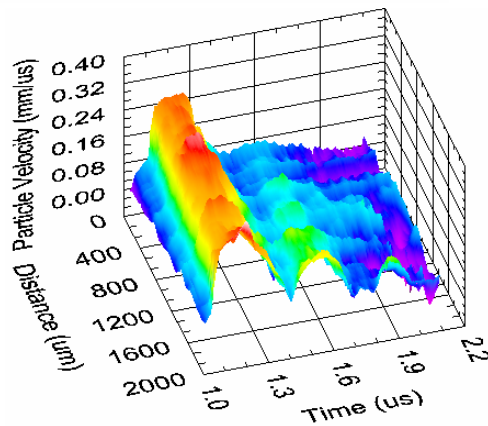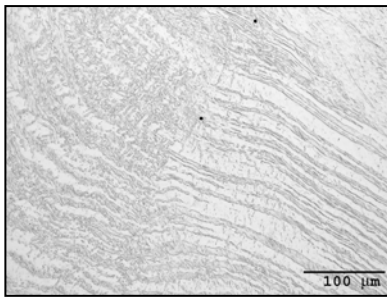
Figure 1.2. Spall signatures for tantalum samples which have been subject to two different preparations.

Second, with this long relay, even a slight rotational motion of a highly specular target will cause strong variations in the intensity delivered to the streak camera aperture. Finally, the speckle inherent to multi-mode fiber-optic delivery is anathema to high-resolution VISAR recording; use of the free-beam laser delivery of light to the target is necessary. In addition, in pulsed-power environments, the positioning of the beam on the line of interest must be finished by remote control means, such as stepper motors with videocamera monitoring.
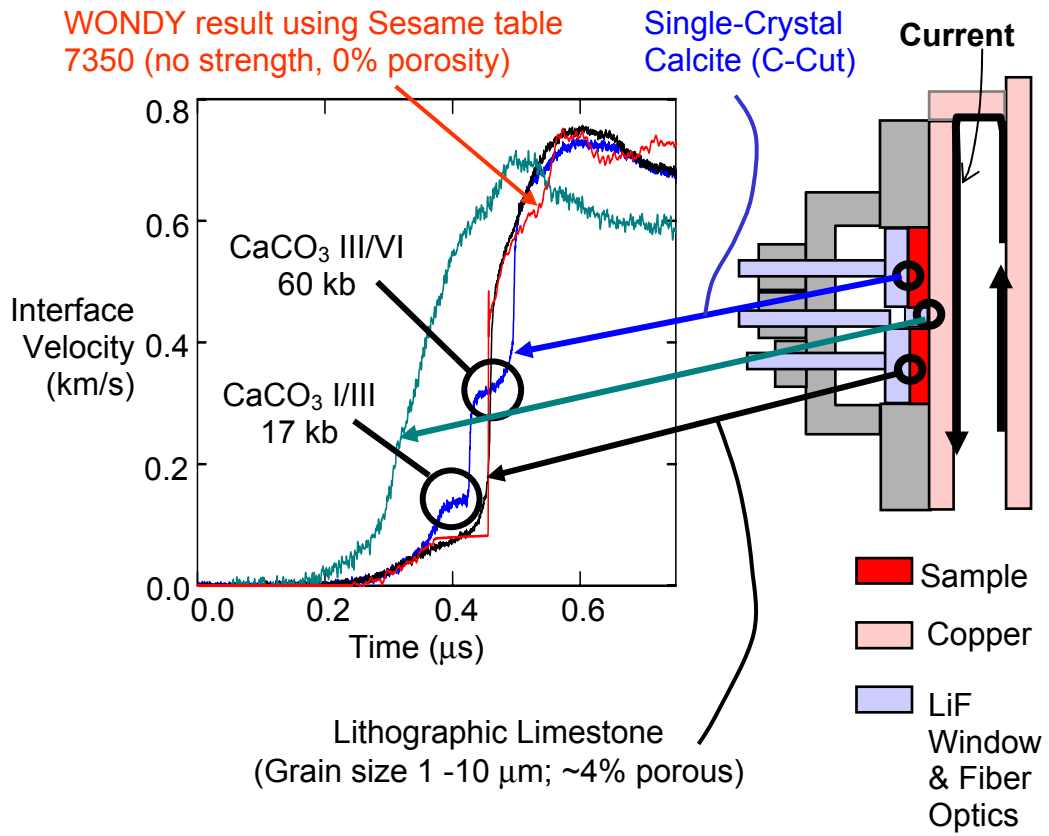
Figure 1.3. Isentropic compression behavior of single-crystal calcite and finely polycrystalline calcium carbonate (Z shot 938).

2.0 Scope of Effort

The following represent the areas of concentration of this study:

- Demonstrate a usable 12 m optical relay and line VISAR system on the benchtop which has 10 micron resolution on a target.

- Prepare a VISAR system at a pulsed power facility with usable 10 micron resolution.

- Consider bonding techniques which may be necessary for bonding samples to ICE panels (e.g. diamond-machined Cu or Al) to allow mesoscale studies. The existing glue-bond methods are not always adequate because of the finite (1 micron) thickness of the glue bond.

- Conduct experiments to demonstrate the implementation of the VISAR system.

2.1. Benchtop development.

A line VISAR system was prepared on the benchtop with the following attributes:

- The velocity-per-fringe (VPF) sensitivity was controlled by selection of glass etalons, in the range from 100 m/s (all etalons used) to 5 km/s (no etalons used). A Wide-Angle Michelson Interferometer (WAMI) was used to precisely position the delay leg mirror and to determine the velocity-per-fringe sensitivity.

- A programmable stage allowed pre-setting positions for the delay leg mirror, providing an easy way of adjusting VPF sensitivities.

- A single Imacon 500 streak camera with 17 mm acceptance slit was positioned above the VISAR table to record the fringe data.

- A 12 m relay was built to study possible lens configurations.

The resolution was verified using a photolithographed test pattern (Fig. 2.1).
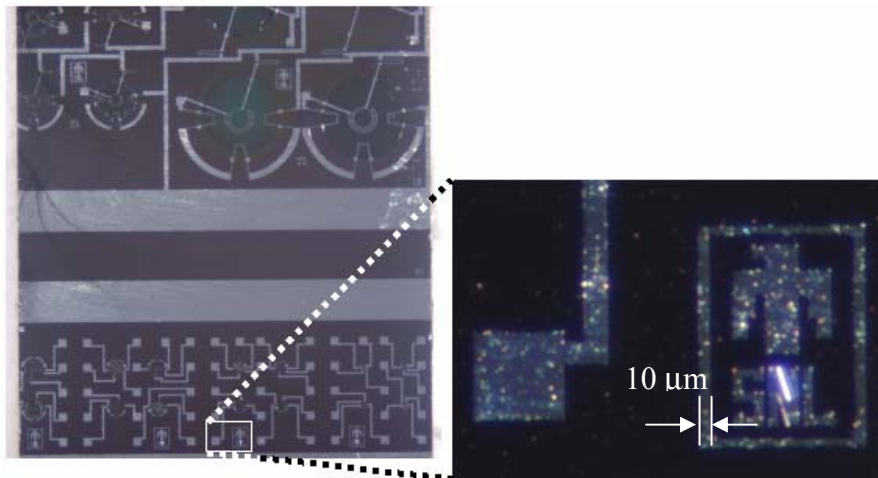
Figure 2.1. Test pattern used for resolution verification

11

2.2. VISAR / Relay construction at pulsed-power facility.

Two VISAR systems were constructed, one for implementation at the Z Facilty (9/10 screenbox), and the other for implementation at the STAR Facility compressed-gas gun.

The system at Z was constructed as an upgrade to an existing line VISAR system in the 9/10 screenbox. Changes included (1) emplacing hardware to accommodate the improved relay optics, and (2) introducing variable velocity-per-fringe (VPF) sensitivity settings. The variable-VPF modification included rearranging optical elements to accommodate a selection of glass etalons and installing an electromechanical system to reproducibly move the delay leg mirror to the proper settings for respective selections of etalons (hence VPF settings). Currently VPF settings from 200 m/s to 4.5 km/s (free surface) are available. This system is operational at the present time, with 10 micron resolution.

The system at STAR was built new. Although it was built to work on the compressed gas gun, with minor modifications it can be used on the other ranges available at STAR. Hence it can be used on systems producing impact velocities of 50 m/s up to 16 km/s. It is functional at the present time with 10 micron resolution and VPF settings similar to those at Z.

As noted before, the resolution is a function of the relay optics. The first lens and mirror are necessarily sacrificed with each shot.

An overall photograph of the system at STAR is shown in Fig. 2.2.
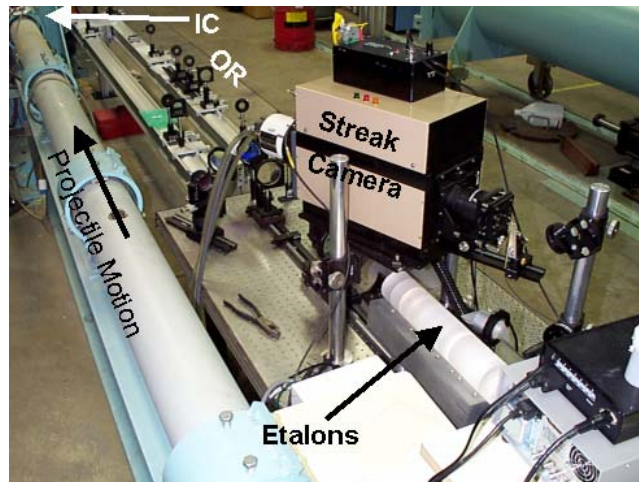
Figure 2.2. STAR HR Line VISAR. VPF sensitivities of 0.1 – 4.0 km/s are available. OR = Optical Relay. IC = Impact chamber.

2.3. Bonding techniques appropriate for mesoscale samples.

Traditionally samples have been incorporated into ICE experiment by one of two methods. They have been bonded to the diamond-turned copper or aluminum counterbores by a low-viscosity adhesive, and compressed in a clamp during curing to give bond thicknesses verifiably less than 1 μm. Alternatively, they have been

constructed as part of the ICE panel. As an example of the latter, aluminum may be studied by constructing an ICE panel of the desired Al alloy with counterbores chosen to be of several appropriate thicknesses.

Under certain conditions, adhesives may not be adequate. In particular, they will not be adequate if (1) the temporal perturbations to the wave introduced by the finite thickness of the glue layer (a low-impedance material) obscure critical wave properties, or (2) lateral variations to the wave introduced by the glue layer obscure similar variabilities in the observed wave produced by sample variations of interest.

We have considered the following alternatives:

- Diffusion bonding appears appropriate for electrodeposited nickel, iron, or copper based samples, such as LIGA materials. The two surfaces to joined must be flat to of order 50 nm rms (typically of diamond-turned surfaces), although greater roughness may be tolerated in softer materials.   For Ni or Cu-based materials, the surfaces are placed in direct contact, then the samples are placed in a press and subjected to a temperature of 650°C and pressure of roughly 14 MPa (2100 psi) for a period of one hour. If both of the parts to be joined have melting points above ~1200°C, a 50 – 100 Å "adhesion" layer of Au or Ti may be sputtered onto one surface prior to the bonding. We used this method for bonding Ni-based LIGA samples to Cu target plates. If these bonding conditions would degrade the sample, this method would not be appropriate. If not, this method used with diamond-turned surfaces provides a <100 Å thick bond layer (a factor of 10 – 50 better than glue bonds).

- Electrodeposition of metallics onto a copper or aluminum ICE panel may be directly made. This is especially appropriate for LIGA samples, which are formed by electrodeposition into PMMA molds made with a synchrotron-radiation (X-ray) based lithography method. Such samples may be plated onto an ICE counterbore [T. Lemp and T. Christenson, personal communication]. For this method, the bond thickness is of the order of a few Å, although epitaxial influences may persist for several microns.

Other methods may also be appropriate, such as:

- Ion-gun assisted growth of samples on an ICE panel may be appropriate for some experiments.

- Magnetic attachment of paramagnetic samples to a magnetized ICE panel.

2.4 Suite of experiments to demonstrate the VISAR systems.

Z Facility: Due to the limited number of shots available at Z, it was decided to demonstrate the system there using already-scheduled shots. Two LLNL tests on HMX and the Heterogeneous Nebula shots were selected based on compatibility with the experiments. These tests were successful in that the alignment and implementation of the line VISAR system with the target samples achieved the desired 10 micron resolution. However, due to the laser failure in one experiment, a streak camera failure in a second, and a shot cancellation due to Z machine failure in a third, it was not possible to record

the line-imaging VISAR data.

Star Facility: A program of eight shots was prepared to provide data on a combination of problems of interest while demonstrating the capabilities of this VISAR. These shots are as follows:

(1) Copper sample with "micropore" subject to shock loading

(2) Copper sample with "micropore" subject to ramp (ICE) loading

(3) Copper sample with "micropore" (different construction) subject to shock loading

(4) Copper sample with "minipore" subject to shock loading

(5) Microweld study: 3-piece Ta-Nb-Ta part with one weld joint and one glue joint, with shock loading accelerating the Ta portions of the target.

(6) LIGA sample bonded to a copper "mesa" with shock loading to assess punching/stamping attributes of LIGA Ni material

(7) LIGA sample bonded to a copper "mesa" with ramp loading to assess punching/stamping attributes of LIGA Ni material

(8) RES material (highly porous copper).

Due to failure of the Imacon 500 streak camera on this system[1], shots 1, 3 and 5 were conducted using a streak camera of more limited spatial resolution. These shots are detailed in Chapter 3. The remaining shots, which await repair or replacement of the streak camera, are shown in Section 4.

---

[1] Depts 1646/1647 have 3 Imacon 500 streak cameras, manufactured by Hadland Ltd. During the course of this study one failed to work out of the box and the other two appear to work intermittently. (The manufacturer's representative was unable to repair them and unwilling to replace them. Negotiations are underway for a resolution.) This problem is responsible for loss of the opportunity to complete these experiments during the course of this LDRD.

3.0 Experimental Results

The results of the three experiments completed in this series are summarized here. The philosophy has been to investigate controlled structures on a scale amenable to investigation by high-resolution line-imaging VISAR.

3.1: Single-pore crushup. Two variations of a small pore were employed. Both employed single-crystal copper supplied by V. Nesterenko, cut from the same boule as the samples used in the investigations of Nemat-Nassar et al. [1998]. Analysis of this sort of problem is described by Tang et al [2000]. Fig. 3.1 shows the first variation on this theme. In this configuration, diamond-machined surfaces (50 nm RMS finish) were mated following the drilling of a 2.8 mil (71 micron) diameter hole approx. 1 mm deep. A clamp was used to hold the parts together. No adhesive was used, so it was necessary to incorporate the clamp fixture into the shot (Fig. 3.1c). After assembly in the clamp fixture, the impact and VISAR surfaces were both diamond-turned to 50 nm RMS finish.
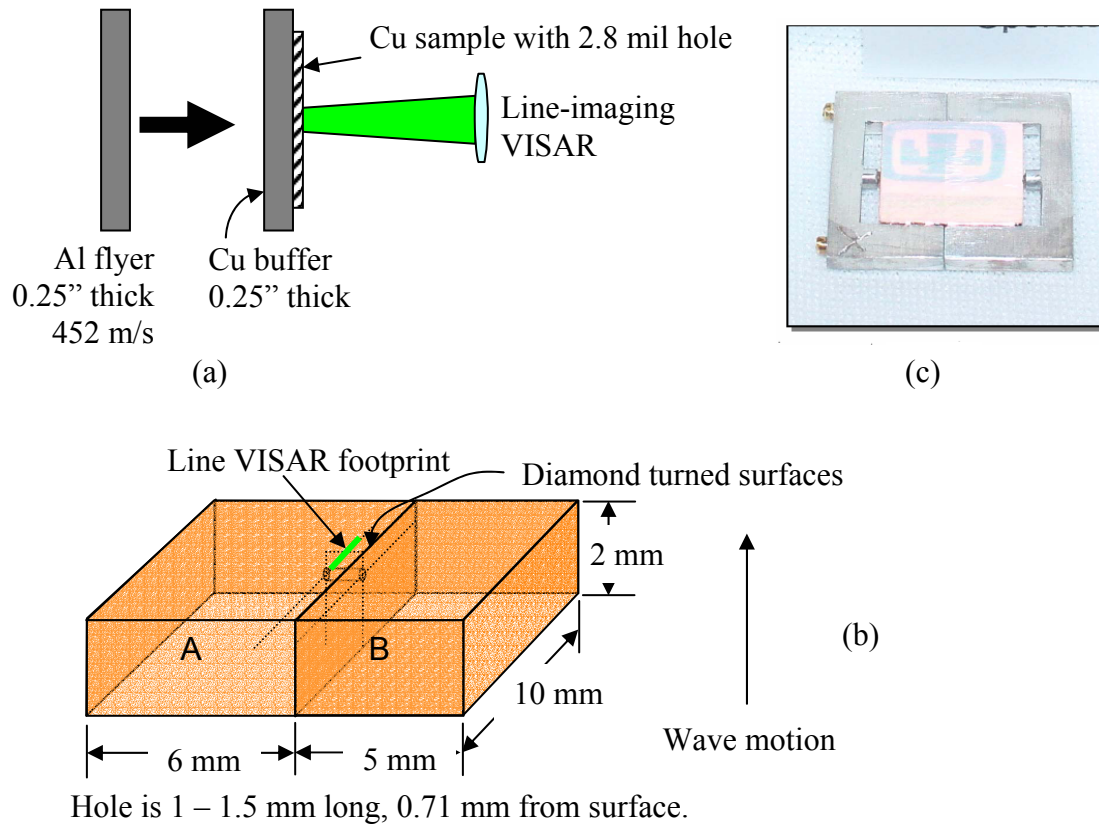
Figure 3.1. (a) General configuration of gas gun micropore configuration. (b) Detail of sample. (c) Photo of sample as-shot, in clamp.
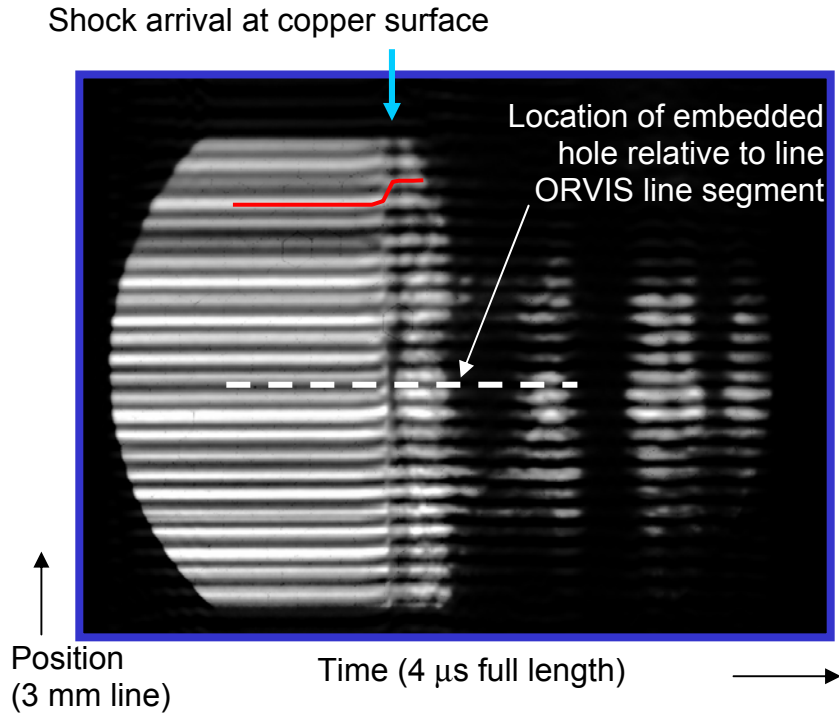
Figure 3.2. Streak camera record for micropore test. A sample fringe is followed past the initial arrival near the top of the image. Reduced results are discussed below.

The distance of the hole from the surface was chosen to be large enough (0.7 mm) that the hole would completely collapse before the release wave from the VISAR surface reached it, on the assumption that the upstream side of the hole would collapse toward the downstream at twice the in-situ particle velocity. With an impact velocity of 0.452 km/s, and an approximate collapse speed of 2×0.133 km/s, the collapse time is estimated as 0.266 µs, slightly less than the two-way transit of a wave at 4.14 km/s (0.34 µs).

Results from this test are shown in Fig. 3.2. Salient features of this streak image are as follows.

Little fringe motion after initial arrival: Upon close examination of this image, it is seen that some deceleration occurs within 0.5 mm of the pore over the first 0.8 µs following the initial wave arrival. This amounts to up to approx. 0.25 fringe (50 m/s). This corresponds to a removal of a cross-sectional area of:

$$\Delta A = \frac{1}{2} \times (50 \ \mu m/\mu s) \times (0.8 \ \mu s) \times (0.5 \ mm)$$

$$= 0.010 \ mm^2 \ (\textit{very crude} \ calculation - more \ careful \ calculation \ below)$$

(where the ½ accounts for the time-averaging of the velocity drop). For comparison, the area of a 71 µm diameter hole is:

$$\Delta A = 0.004 \ mm^2$$

In other words, our crude estimate of lost pore volume is high by 150% for this experiment.

A formal reduction of these VISAR data is discussed below (Fig. 3.5), giving approximately the same estimate of the lost pore volume.

Large contrast: There is a marked loss of light over large areas. The initial reflecting surface was extremely specular, (50 nm RMS) and the relay system provides a sensitive angular-acceptance filter. In other words, a small change in surface tilt can cause a marked change in intensity returned from that region of the sample to the streak camera.

Symmetric appearance of streak image: Both light amplitude and deduced velocity amplitudes show a symmetric appearance about the location of the initial pore.

A CTH [McGlaun et al, 1990] modeling of this problem gives results shown in Fig. 3.3. The velocity variations are comparable to those noted above: approximately 50 m/s on the surface near the pore over an interval approximately 0.3 mm half-width and a time duration of 0.15 µs. Structures at a later time (beginning approximately 0.9 µs after the shock enters the sample) appear to be related to edge effects from the sample boundary rather than the pore.
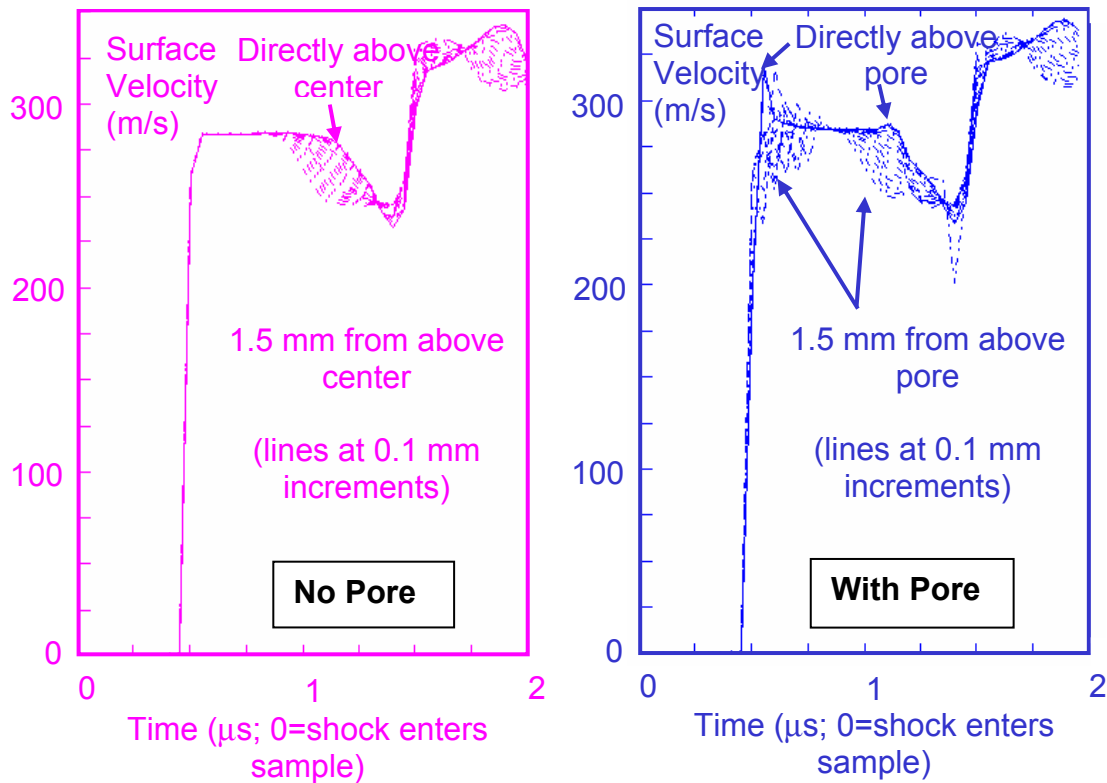
Figure 3.3. 2-d CTH simulation of micropore problem.

A reduction of the streak camera image to velocity/position/time space is shown in Fig. 3.4. The overall amplitude of the plateau velocity (280 m/s) agrees with calculations, as does the time lag (0.7 µs) between the initial wave arrival and a major pullback. As well, a small-amplitude (20 m/s) valley at the position of the pore (1200 µm) is observed. However, with the velocity per fringe utilized (200 m/s), this must be accepted as imprecise.

17
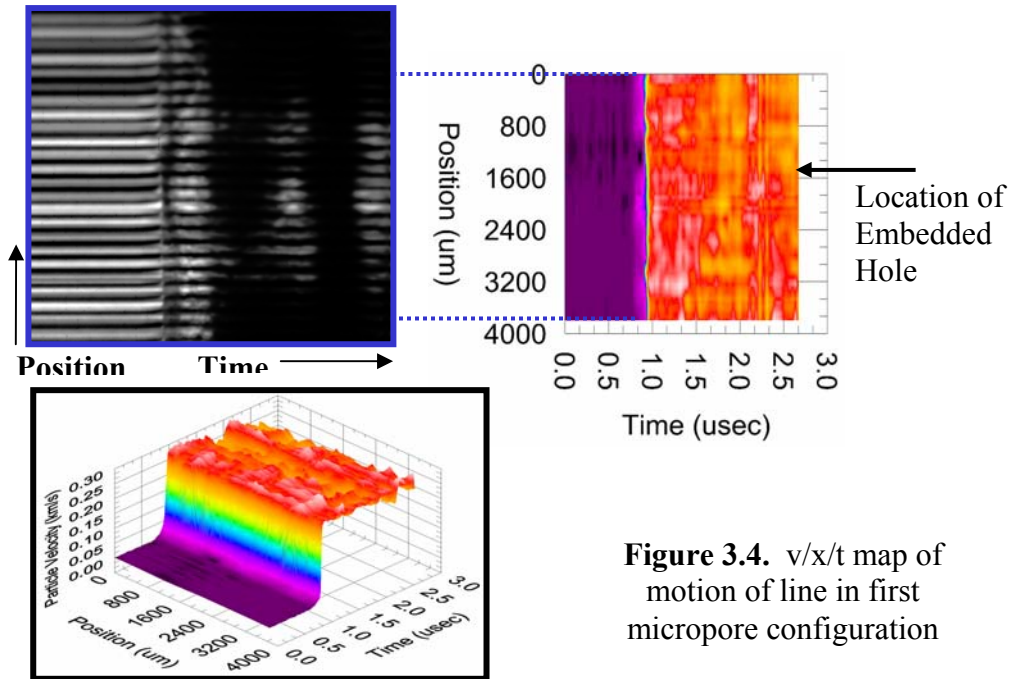
Figure 3.4. v/x/t map of motion of line in first micropore configuration

In an effort to assess how the variations of the v/x/t surface shown in Fig. 3.4 are related to the micropore collapsing, we integrated velocity at each position x to obtain displacement. The result is plotted in Fig. 3.5 (with the average value of 0.459 mm subtracted out). Integrating the below-average displacement in the shaded area to obtain the pore cross-sectional area yields a value of 0.0093 mm^2. The position of the hole only corresponds moderately well to the position of the apparent crush volume on the integrated plot. Integrating only to 0.4 µs after wavefront arrival (average displacement of 0.157 mm) yields a collapse volume of 0.0015 mm^2, suggesting that the crush-up takes more than the nominal 0.26 ms.
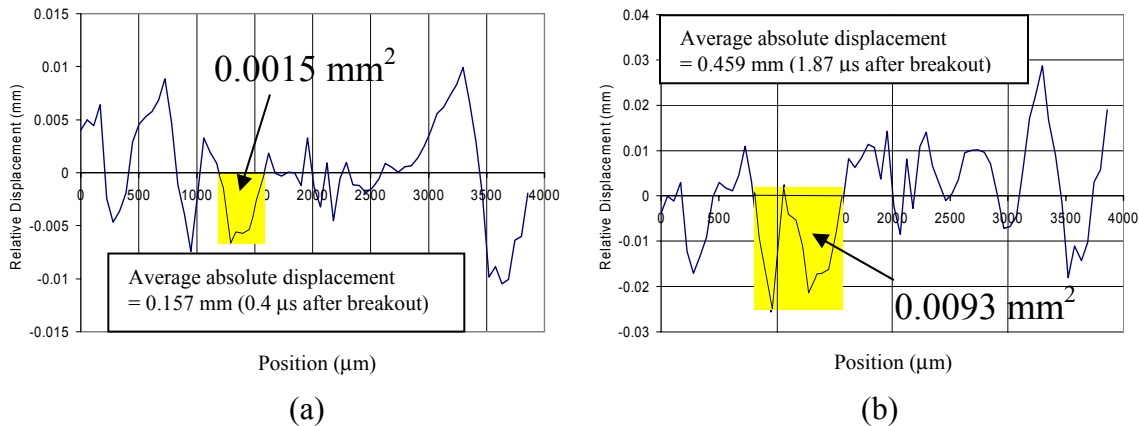
Figure 3.5. Displacement as a function of position; (a) integrated 0.4 µs after wave arrival; (b) integrated to end of recording. The embedded hole is at 1500 µm. (Nb. this represents the surface profile along the imaged line at 0.4 µs or 1.87 µs after breakout)

18

The second configuration, shown in Fig. 3.6, utilizes a carefully emplaced slot in a diamond-turned surface as a "hole." Results from this test are shown in Fig. 3.7. The streak camera records show an intricate, symmetric appearance of the streak image. Although there is little fringe motion after the initial arrival, the contrast patterns are likely to convey additional information.
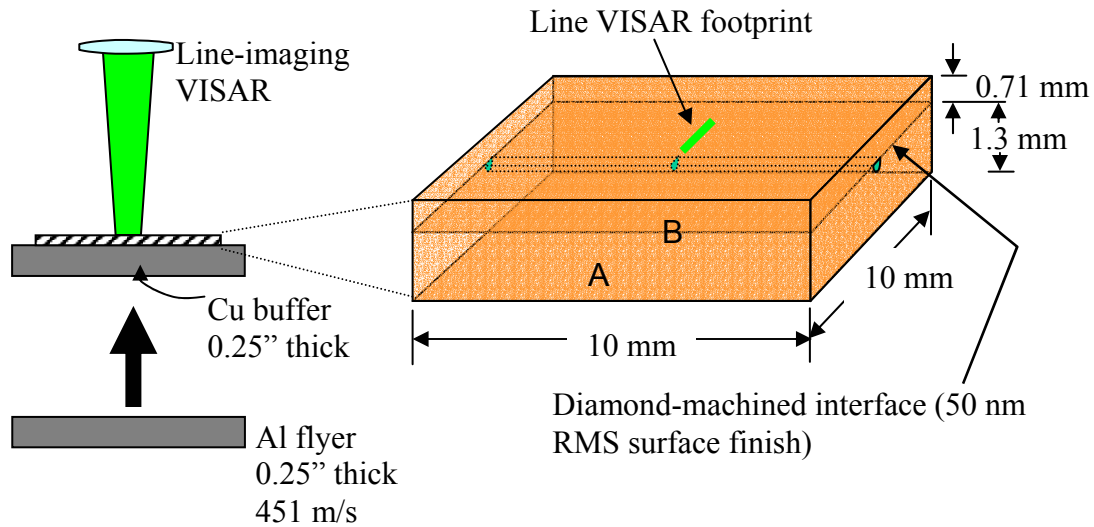
Figure 3.6. Configuration of second type of "micropore".

As with the previous configuration, diamond machined surfaces were utilized to provide "disappearing interfaces," i.e. interfaces so closely mated that their effect on the experimental results is negligible.

Results were integrated in the same manner as described for the first micropore test; results are shown in Fig. 3.8. For this case, the volume of the hole appears to be underestimated. However, the cross-sectional volume of the actual hole is not as well known for this case as it was for the first micropore experiment.
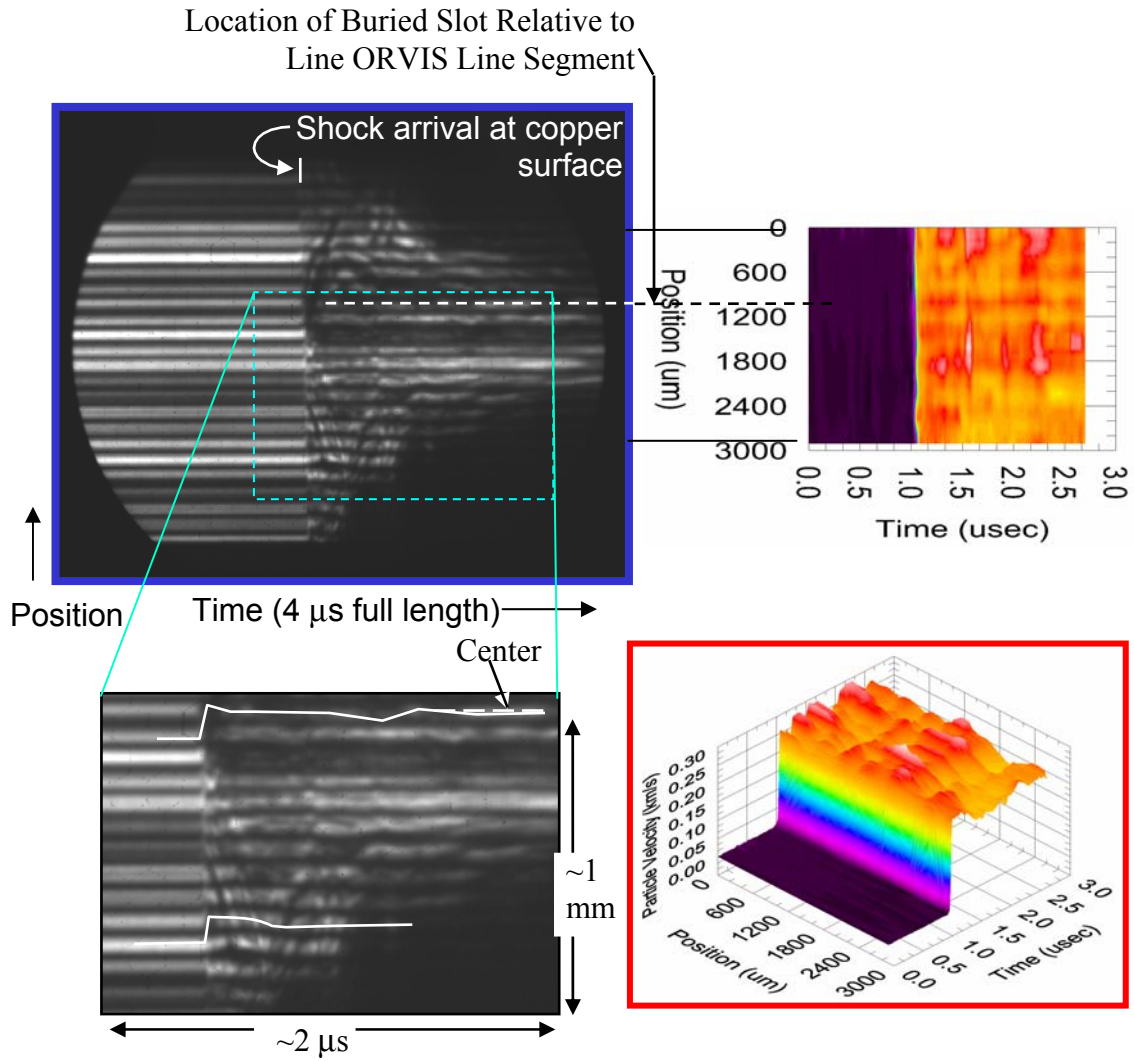
Figure 3.7. Results from second variation of micropore.
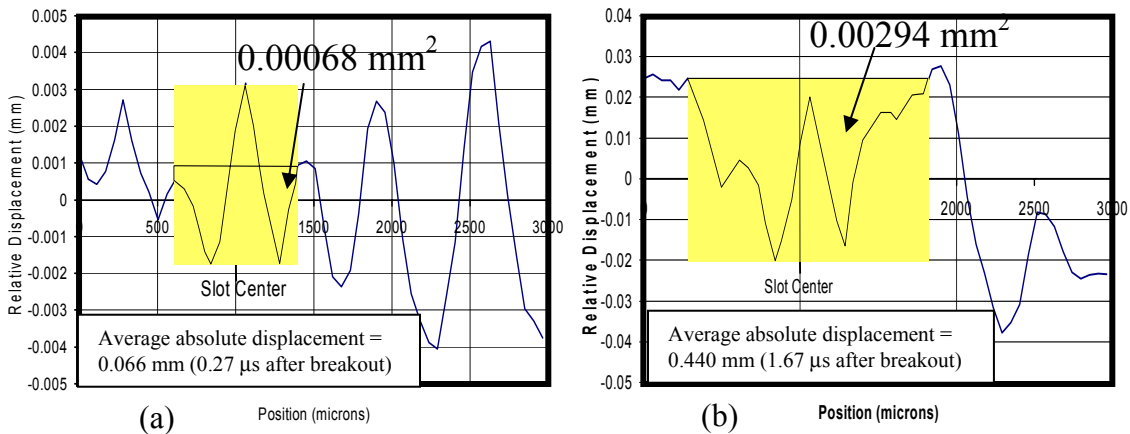
Figure 3.8. Displacement as a function of position; (a) integrated 0.4 μs after wave arrival; (b) integrated to end of recording. The embedded hole is at 1000 μm..

3.2: Weld/Glue Failure.   A third configuration, shown in Fig. 3.9, contrasts failure of a weld with failure of a glued boundary. A slot machined in the buffer provides for a shearing force on the sample at the bonded (welded or glued) surfaces. The prediction is that there will be a ductile element to the breaking of the weld, while the glue bond (Hysol epoxy) will easily shear.   The glued and exposed surfaces were diamond machined.

Similar sample, although with two welds and no glue bonds
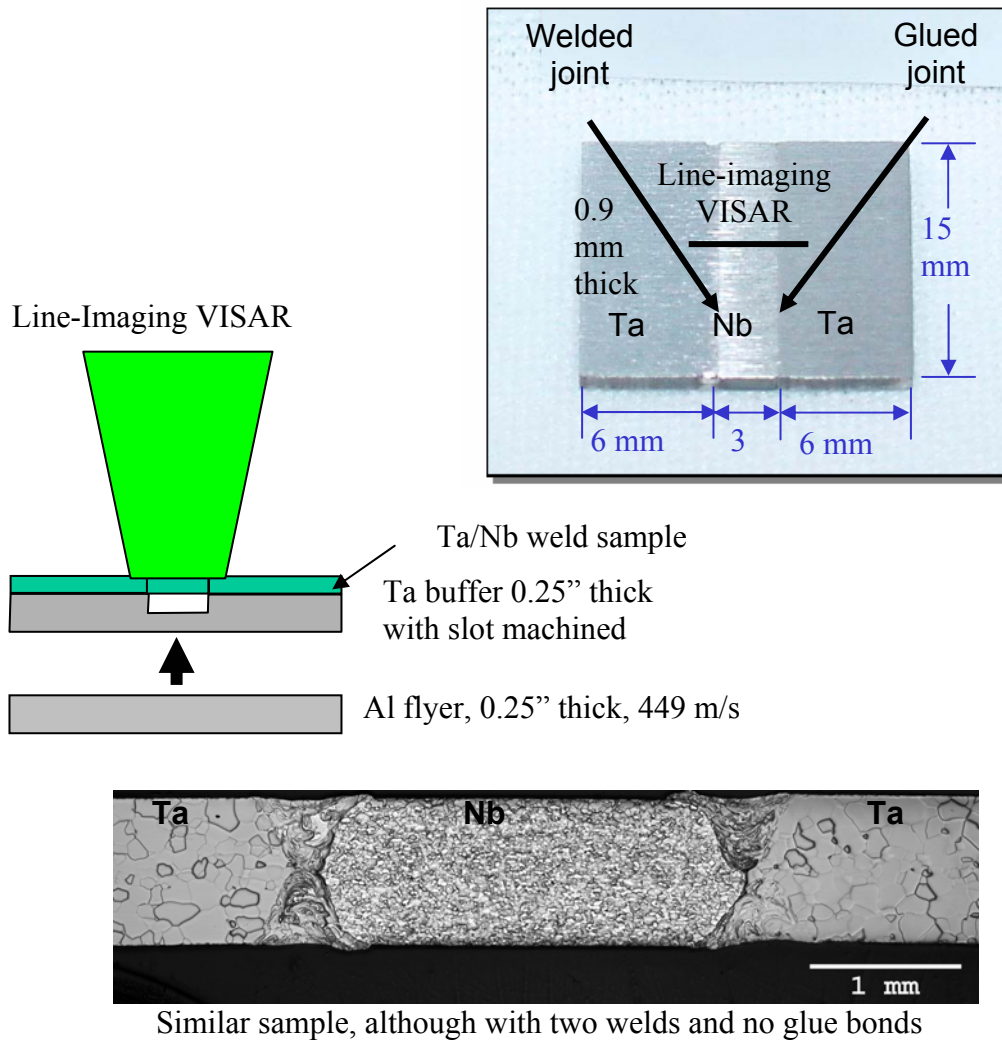
Figure 3.9. Weld/glue configuration.

Results are shown in Figure 3.10. The weld boundary shows a dramatic drop in returned light amplitude, corresponding to distortion of the metal adjoining the boundary. However, light amplitude remains relatively stable adjacent to the glued boundary, indicating that little distortion occurred.

Location of interfaces between tantalum and niobium

Glue

Weld

Position (6 mm line)

Time (4 µs full length) ⟶

❶ Acceleration
❷ Small-scale velocity oscillations
❸ Difficult to resolve details (surface distortion)
❹ Substantial velocity dispersion (loss of fringe contrast) in this region
A Glued (light amplitude at boundary stable)
B Welded (light amplitude at boundary drops dramatically)
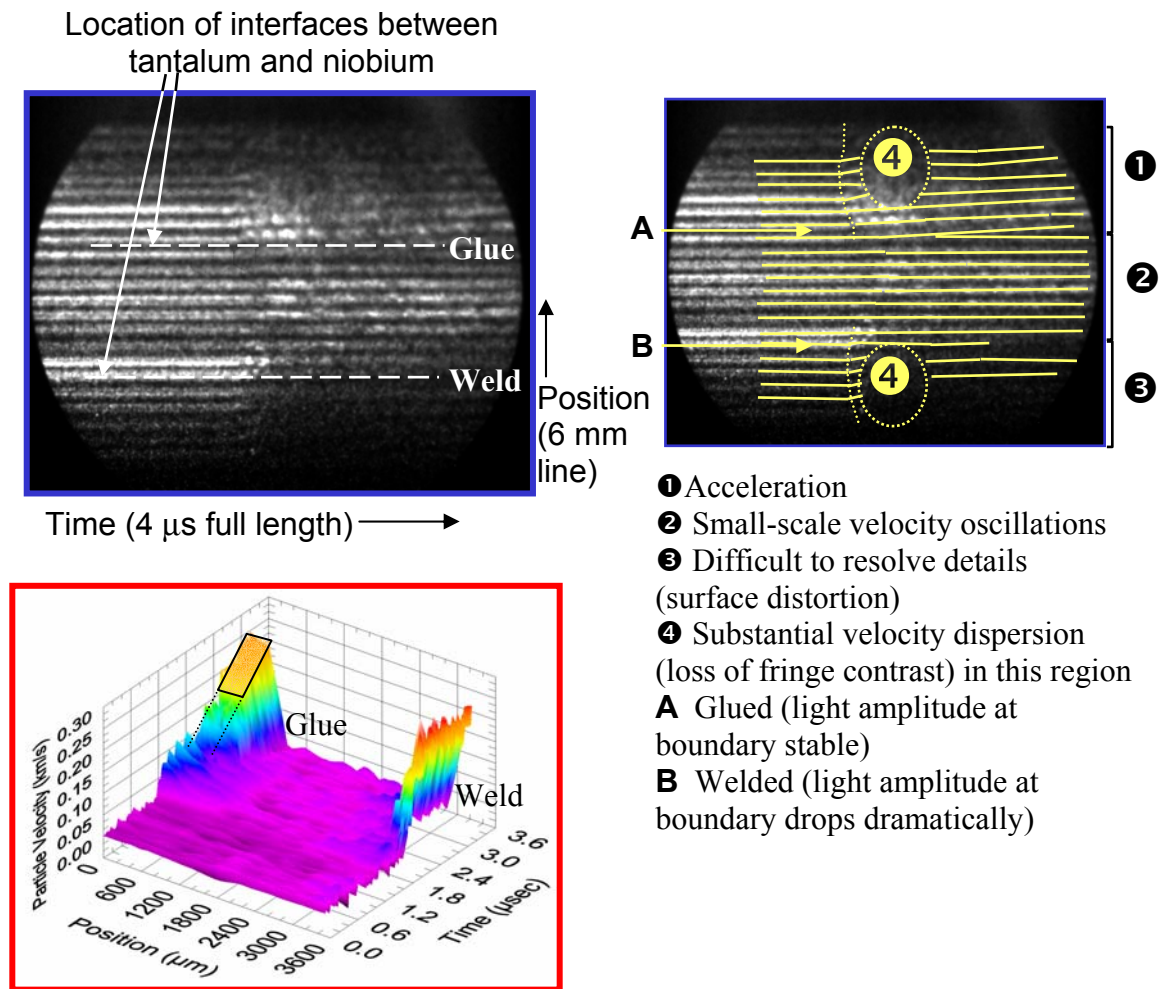
Figure 3.10. Results for weld/glue configuration.

The weld boundary shows a dramatic drop in returned light amplitude, corresponding to distortion of the metal adjoining the boundary. However, light amplitude remains relatively stable adjacent to the glued boundary, indicating that little distortion occurred.

3.3: Experiments pending. The experiments which were not been completed (due to the unavailability of the streak camera associated with the high-resolution system at STAR) are shown in Fig. 3.11. These will be executed when the high-resolution streak camera is available. Included are two shots assessing the folding properties of LIGA materials [Hruby et. al., 1999], one with a larger pore in soft copper, and one on a highly porous copper (flame spray material). One additional shot in the configuration of the first copper micropore shot is also planned for execution.

22
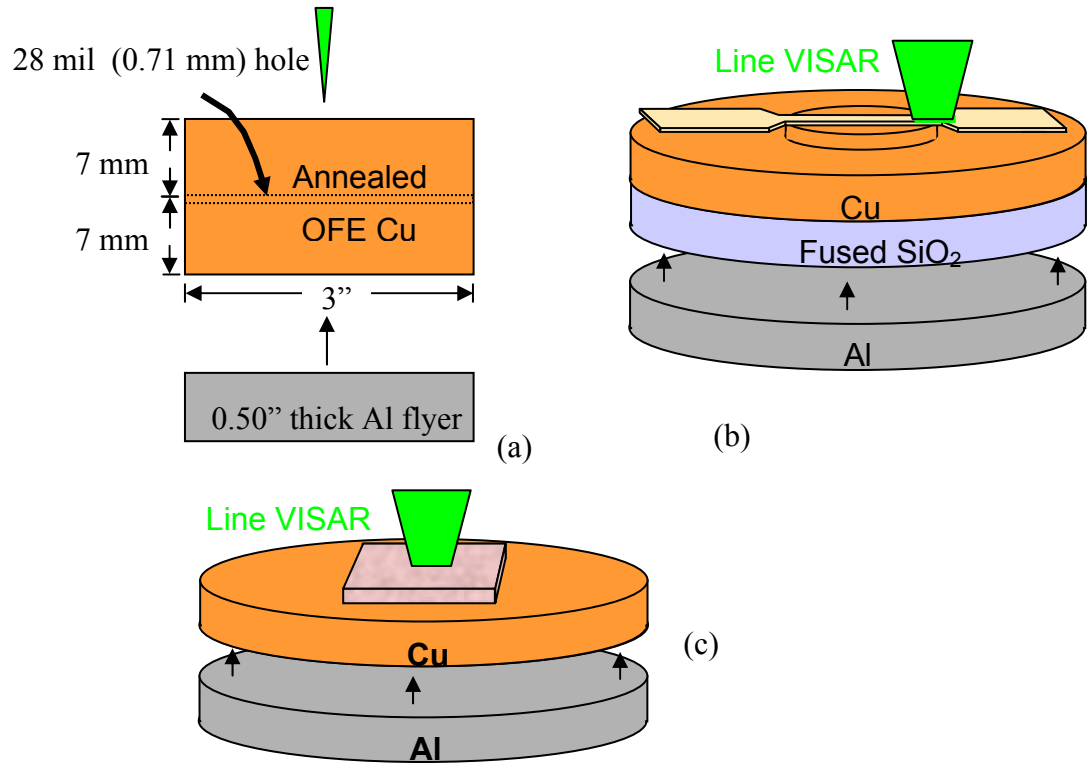
Figure 3.11. Experiments pending. (a) Copper pore 10x larger than micropore (b) LIGA sample across edge (2 shots: ramp and shock loading; ramp loading variant shown); (c) Flame spray material (highly porous copper).

4.0 Overall Summary

During the course of this study, we have designed and constructed two line-VISAR interferometers with ~10 micron maximum spatial resolution. One is at the Z facility (9/10 screenbox) and one is at the STAR facility (gas gun range). Both have the capability of user-selectable sensitivity (velocity-per fringe settings), facilitated by a programmable stepper motor positioning of the delay-leg mirror. We demonstrated the requisite resolution on two Z tests, although unrelated issues prevented the actual measurement of shot waveforms at Z.

We constructed a series of eight gas-gun tests to utilize the high-resolution line-imaging VISAR at STAR. These included carefully controlled assessments of pore collapse in copper, LIGA stamping measurements, the dynamic compression of highly porous copper, and a comparison of the dynamic failure of a Ta-Nb weld and a Ta-Nb glue joint.   Due to a progressively more intermittent functioning of the Imacon 500 streak camera in early qualification tests of the STAR system, three of these tests were performed on a lower-resolution VISAR system. The other tests were not executed and await the repair/replacement of the streak camera.

Among the tests executed, we find that the collapse volume of a pore can be estimated to within a factor of two. Further improvements are possible with more careful analysis. Collapse rates may also be measured; these are found to be lower than predicted for low-strength copper. Fringe intensity information may convey useful tilt information for these systems because of the long relay system and highly specular surfaces used. Distortion of surfaces adjacent to a failing weld and glue joint were monitored. Although the glue joint clearly broke, the behavior of the weld was more difficult to infer. It appears that material distortion was extensive near the weld joint.

Diffusion bonding is appropriate for some types of bonds, where glue bonds would result in excessive ramp time, wave heterogeneity or other undesirable perturbations. Magnetic bonding or plating directly onto ICE panels are also viable bonding schemes for certain types of experiments.

References

Chhabildas, L. C., W. M. Trott, W. D. Reinhart, J. R. Cogar and G. A. Mann, Incipient spall studies in tantalum – Microstructural effects, pp. 483-486 in Shock Compression of Condensed Matter – 2001, M. D. Furnish, N. N. Thadhani and Y. Horie (eds.), AIP Press, 2002.

Hemsing, W.F., Matthews, A.R.; Warnes, R.H.; George, M.J.; Whittemore, G.R, VISAR: Line imaging interferometer, pp. 759-767 in S. C. Schmidt et. al, *Shock Compression of Condensed Matter – 1991*, North-Holland, 1992.

Hruby, J, A. M. Morales, D. R. Boehme, J. S. Krafcik, W. D. Bonivert, S. K. Griggiths, R. H. Nilson and B. V. Hess, LIGA Micromaching: Infrastructure establishment, Sandia National Laboratories report, SAND99-8228, 1999.

Ivanov, B. A. and A. Deutsch, The phase diagram of $CaCO_3$ in relation to shock compression and decomposition, *Phys. Earth and Planetary Interiors* **129**, 131-143, 2002.

McGlaun, J. M. S. L. Thompson and M. G. Elrick, CTH – A three-dimensional shock wave physics code, *Int. J. Impact Engrg,* **10**, 351, 1990.

Nemat-Nasser, S., T. Okinaka and V. Nesterenko, Experimental observation and computational simulation of dynamic void collapse in single-crystal copper, Mat. Sci. & Engrg. A (Structural Materials: Properties, Microstructures and Processing); **A249**, 22-29, 1998. See also Nesterenko, *V. Phil Mag. A,* **78** (no. 5), 1151-1174, 1998.

Tang, Z.P., Wenyan Liu; Horie, Y, Numerical investigation of pore collapse under dynamic compression, pp. 309-312 in M. D. Furnish, L. C. Chhabildas and R. S. Hixson, *Shock Compression of Condensed Matter - 1999*, AIP Press, 2000.

Trott, W. M., M. D. Knudson, L. C. Chhabildas and J. R. Asay, Measurements of spatially resolved velocity variations in shock-compressed heterogeneous materials using a line-imaging velocity interferometer, pp. 993- 996 in M. D. Furnish, L. C. Chhabildas and R. S. Hixson, *Shock Compression of Condensed Matter - 1999*, AIP Press, 2000

Xu, X. and N. Thadhani, 2002: These Ni-Ti samples were prepared at Georgia Tech by dynamically compressing an intimate mixture of Ni and Ti (6:4 weight ratio; grain size 40 – 150 microns) powders to 5 – 10 GPa by gas-gun planar impact. For details, see X. Xu, Shock consolidation and reaction synthesis of NiTi intermetallic, Ph.D. thesis, Georgia Institute of technology, 2001.

Appendix

Sub-System Overviews
(Excerpt from Operations Manual for
STAR Line VISAR System)

J.W. Podsednik, 1647

This Appendix provides a brief overview of each sub-system's function and the overall system as a whole.

    A. Beam Modulator
    B. Line Shaping Optics
    C. Target Illumination
    D. Relay Lens Leg
    E. Interferometer
    F. Streak Camera and Impulse Dot / Comb Generator

A.1 Beam Modulator

An optoacoustic beam modulator is used to "slice" a user-defined pulse width (typically, a few hundred microseconds) out of the CW Coherent Verdi laser beam. This modulation is created by interactions with sound waves in a solid. As an acoustic wave passes through a solid, it alternately raises and lowers the pressure, which, in turn, changes the refractive index of the solid. Light waves passing through the solid material see these variations in refractive index as a series of layers, much like a diffraction grating. Both interference and diffraction effects combine to scatter light from the "acoustic grating" at an angle that depends on the ratio of the wavelengths of light and sound in the solid medium. That portion of the main beam, which is deflected at this angle, is the pulsed beam, which is used to illuminate our target.

Modulating the CW laser beam has several benefits:

    1.) Ease of intensity adjustment for alignment by simply varying the repetition rate of the delay generator,

    2.) Providing the ability to somewhat "freeze" vibrating fringes by tuning the repetition rate of the delay generator to the approximate vibration frequency, and

    3.) Minimizing the amount of light exposure on the target, thus reducing the exposure time of light on the recording medium (film, CCD, etc.).

The beam modulator is easily setup and adjusted. With the laser at low power, the

beam modulator is inserted into the beam path near the output of the laser. An input pulse from a delay generator is used to turn the modulator "on". Currently the A ∏ B output is used to trigger the modulator. Typically, the modulator is only on for a couple of hundred microseconds at most. This A ∏ B output is then fed into signal generator for the modulator and again, relayed to the modulator itself.

A.2 Line-Shaping Optics

The line-shaping optics is basically a four-lens pair of various lens types. See Figure A1. The first lens in the chain is a spherical lens, in this case, with a focal length of 200mm. The purpose of this particular lens is to focus the collimated laser to a very small diameter spot. It is this small spot that you want to image (in one dimension) to the target in order to get a thin line. The second and third lenses are cylindrical. They are both oriented in the same manner to provide a vertical line orientation. These two lenses operate on the beam diverging from the small spot created by the first spherical lens.
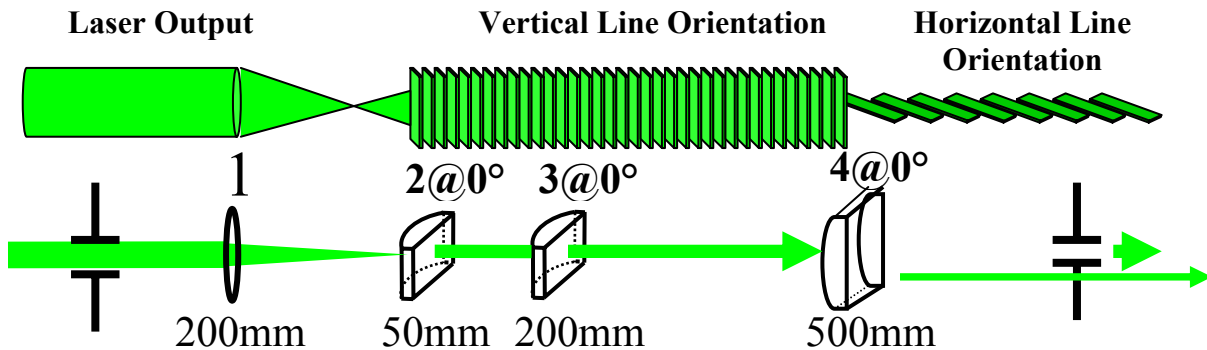
Figure A1. Line-Shaper Layout

Lens four is also cylindrical, but its orientation is such that its curvature is ninety degrees of the second and third lenses. This is shown by the figure above. This brings to a focus the line in a single dimension, but now, it's oriented in the horizontal manner. This is typically the desired line orientation projected onto the target.

This optical scheme provides the user with many capabilities when it comes to choosing desired line dimensions. The distance between lens one and lens four can be adjusted to vary the line thickness. Ideally, you want the thinnest line possible on the target surface. The following equation offers this condition:

The distance between lens 1 and lens 4= 2XFL of lens 4 + lens 1 FL; in the above case this distance will be 1200mm.

This distance between these two lenses will yield the thinnest line possible on the target, given the next condition is also true:

The distance between lens 4 and target= 2XFL of lens 4; in the above case, this distance will be roughly 1000mm.

Lens two and lens three are commonly placed on a smaller rail separate from the other lenses. This is so that the distance between the two lenses does not change. By moving these two lenses in conjunction with each other, you cause lens two to catch the focused spot at a different point within that focus, or waist. Doing this allows the lenses (two and three) to image a larger spot or a smaller spot, which, in turn, images a longer or shorter line onto the target. Lens four can be adjusted slightly to accommodate the desired thickness of the line onto the target. As stated before, you most commonly wish to obtain the thinnest line possible on the target.

Another capability the cylindrical lenses buy is the fact that the orientation of the line onto the target can very easily be rotated to accommodate almost any target orientation. In short, the line can be projected as vertical onto the target rather than horizontal. For example, Figure A1 illustrates a horizontal line being projected to the target. To rotate that line such that it may be vertical on the target, you simply rotate each of the three cylindrical lenses ninety degrees. Any line orientation can be achieved. One important thing to note however, the line will only be properly imaged if lens four is exactly ninety degrees of lens two and lens three.

A.3 Target Illumination

The illumination of the target is very closely tied to the line-shaping optics. Once the cylindrical lenses establish the line dimensions, the line must now be relayed to the target surface. The line is put through the rear surface of a 50% beam splitter, shown below in Figure A2. The line then travels through a window, usually made of glass, onto a mirror oriented at forty-five degrees.
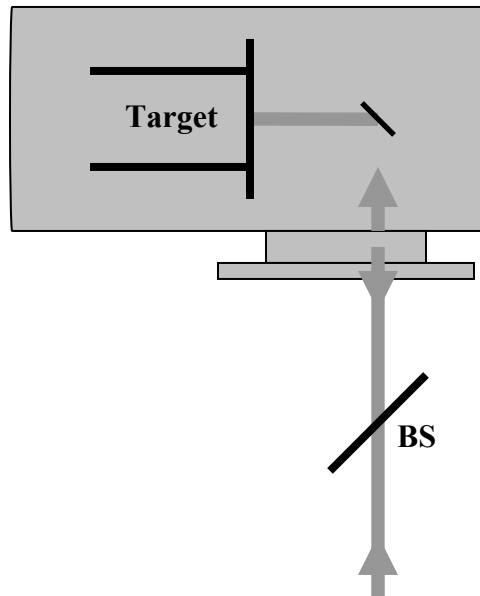

Figure A2. Line projected into Target Chamber

The line is reflected off the mirror and onto the target surface. Figure A3 shows the line on a sample target using the standard, horizontal line orientation
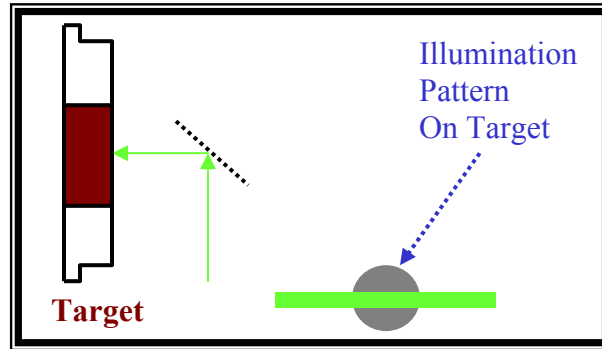

Figure A3. Standard Line Orientation on Target

This line orientation is heavily dependant on the target configuration, and what type experiment is being done. The above sample illustrates a sample target (the gray disk) with a thin, horizontal line placed across it. The part of the experiment that we really care about is the image that is reflected off the target surface. The amount of signal (reflection) off the target surface depends strongly on the surface itself and how it is prepared (whether or not it is specular or diffuse). For the purpose of the system explanation, we will assume that the surface is rather specular, and that reflected light is not a concern. The reflection is caught by the mirror and relayed back down its original input path to the beam splitter. The reflection off the front surface of the beam splitter is then directed towards a 1000mm collection lens and the lens relay leg. This is shown in Figure A4.
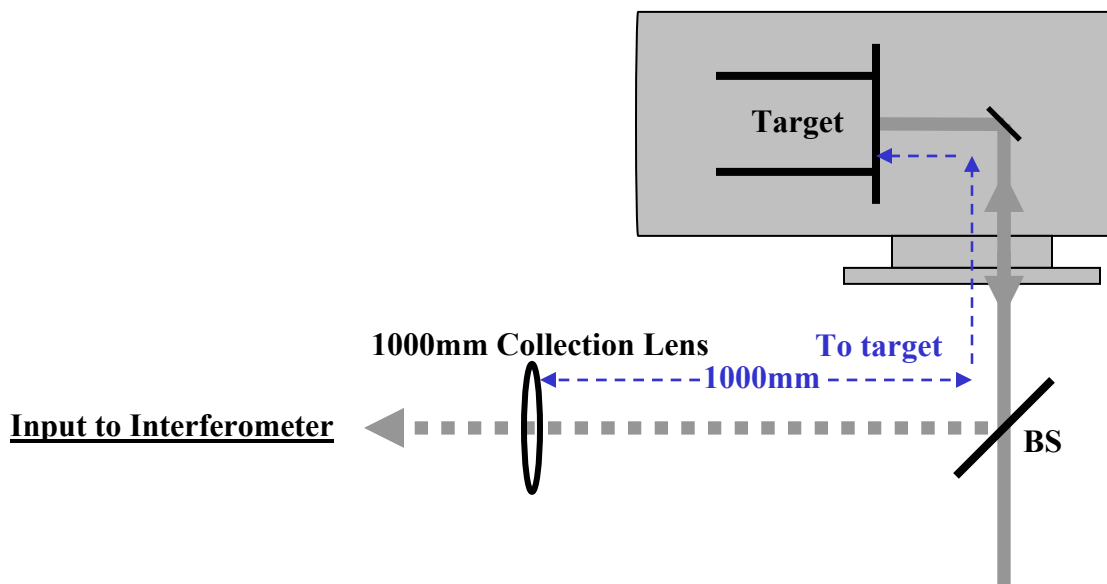

Figure A4. Reflection Off Target to Relay Leg

The line-shaper is basically a four-lens pair of various lens types. These are shown in Figs. A5 and A6. The first lens in the chain is a spherical lens with a focal length of 200mm. The purpose of this particular lens is to focus the collimated laser to a very small diameter spot. It is this small spot that you want to image (in one dimension) to the target in order to get a thin line. The second and third lenses are cylindrical. They are both oriented in the same manner to provide a vertical line orientation. These two lenses operate on the beam diverging from the small spot created by the first spherical lens. Lens four is also cylindrical, but its orientation is such that its curvature is ninety degrees of the second and third lenses. This brings to a focus the line in a single dimension, but now, it's oriented in the horizontal manner. This is typically the desired line orientation projected onto the target.
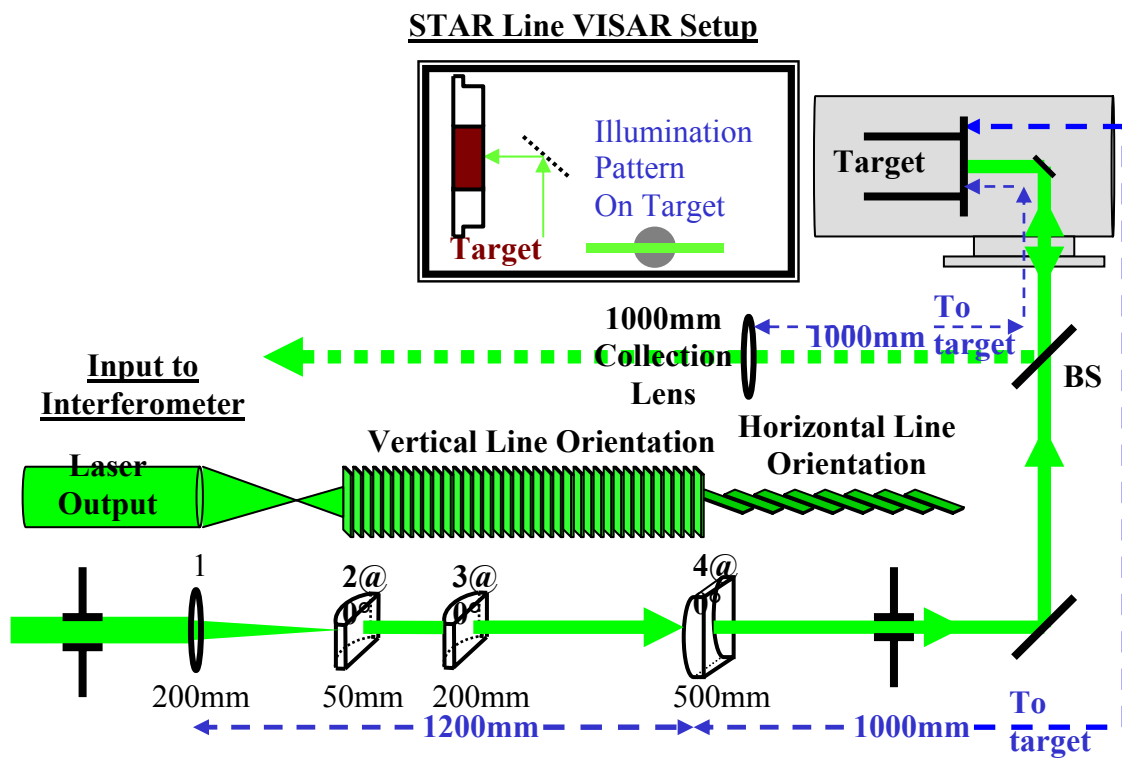
Figure A5. Line Illumination Optics

Figure A6. Line Illumination Optics (Photo)

The line is first reflected off the turning mirror, and put through the rear surface of the 50% beam splitter. The line then travels through the gun port, made of glass, onto a mirror oriented at forty-five degrees. The line reflection is caught by the tank mirror and relayed back down its original input path to the beam splitter. The reflection off the front surface of the beam splitter is then directed towards a 1000mm collection lens and the lens relay leg. This is shown Figure A7.

Figure A7. Turning mirror and beamsplitting optics (Photo)

A.4 Relay Lens Leg

The lenses in the relay leg serve two primary purposes. The first is to simply relay the image down the rail to the interferometer, and the second is to help alter the magnification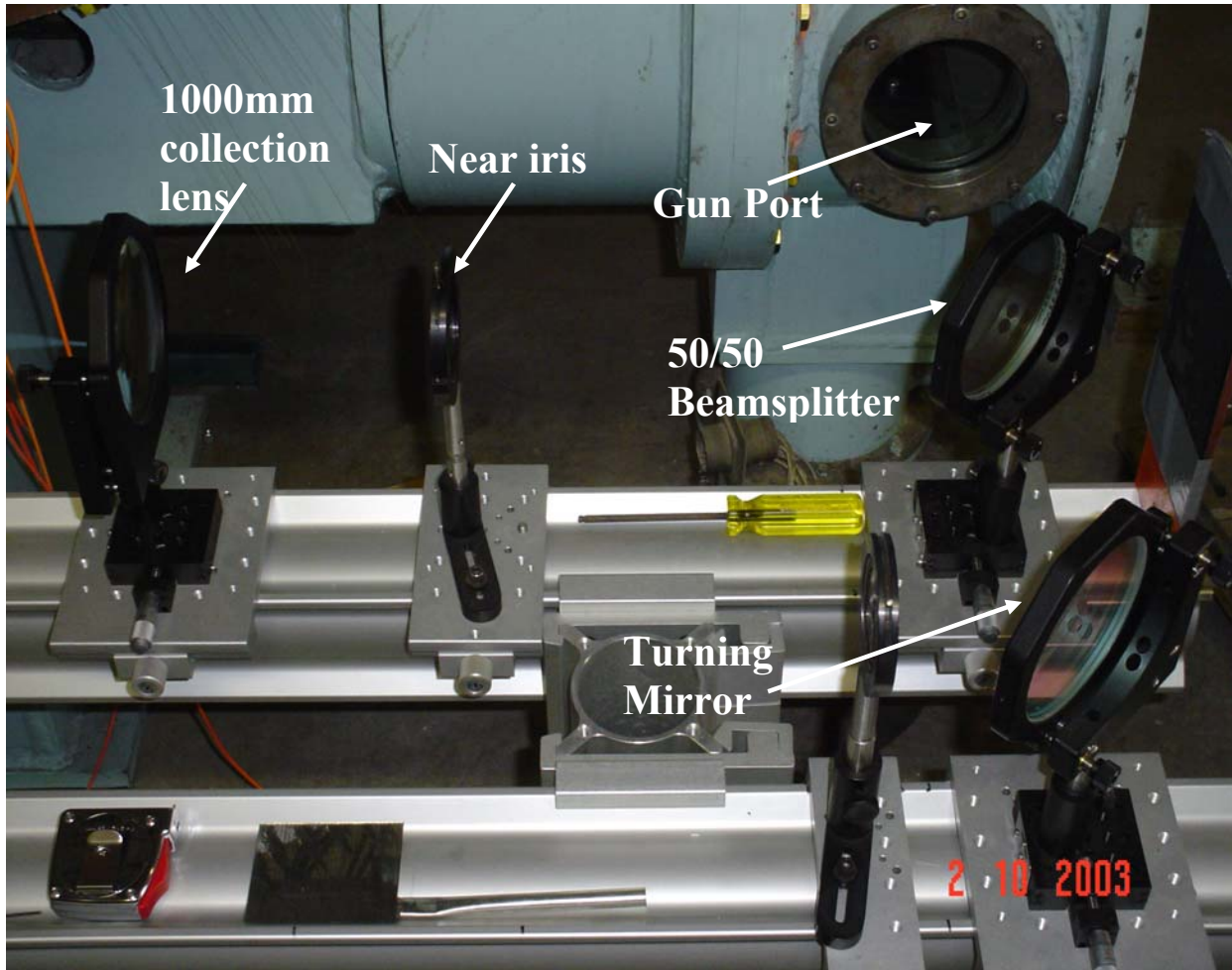 of the image. Once the reflected image is caught and turned by the beam splitter, it encounters the first, and quite possibly the only, optical component in the relay leg. This component is a 1000mm FL length lens as shown, again, in Figure A4. It is desirable to collimate this image, as it will diverge once its distance from the target surface increases (more so for a diffuse surface than a specular one). The collection lens will collimate this image when it is set its focal length away from the target surface, in this case, 1000mm. With only this lens in the relay leg, the default magnification for the imaging system (relay lenses, and interferometer input lenses) is approximately +10. For example, if you wanted to exactly fill the 18mm streak camera slit, and the system's magnification is set at +10, then you would want to project a 1.8mm line onto the target surface.

The system magnification can easily be adjusted by the addition and proper placement of other relay lenses (up to three) along the relay rail. There is a spreadsheet designed to help the operator achieve the desired magnification. It will help tell you, which lenses to choose, and also, where to put them.

The final two lenses in the relay leg are the input lenses to the interferometer. These are designed to complete the imaging scheme and provide somewhat of a "down-collimation" effect. It is imperative that these two lenses be aligned to provide that the image travels directly down the interferometer axis. The fringe field depends on this alignment, and these two lenses must be aligned properly.

A.5 Interferometer

The interferometer is a very useful tool for measuring particle velocity distributions under dynamic shock loading. This tool takes advantage of an optical phenomenon known as interference, which lies in the wave nature of light. When two light waves come together, they add in amplitude. If both waves have their peaks and valleys at the same point, the sum of the two light waves is a wave with larger amplitude, producing a bright spot called "constructive interference". However, if the peak of one light wave comes at the same point as the valley of the other, the negative amplitude of one adds to the positive amplitude of the other. If the two waves have equal amplitudes, the result is a null point, with zero amplitude. This "destructive interference" gives the dark stripe, or void, in an interference pattern.

Now, take for example, Fig A8. This is a simple schematic of the interferometer used in the system. Our image is injected into the interferometer using the pair of periscope mirrors at the table input. The image is down collimated using L1 and L2. The image is then split into two beams of equal intensity by the 50/50 beam splitter. These are also shown in photos of the interferometer (Fig. A9)
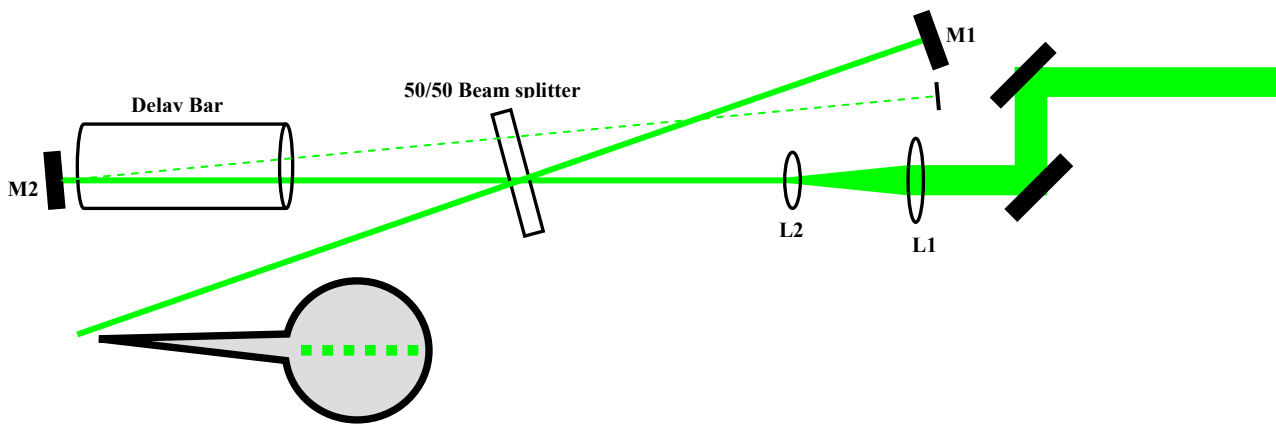

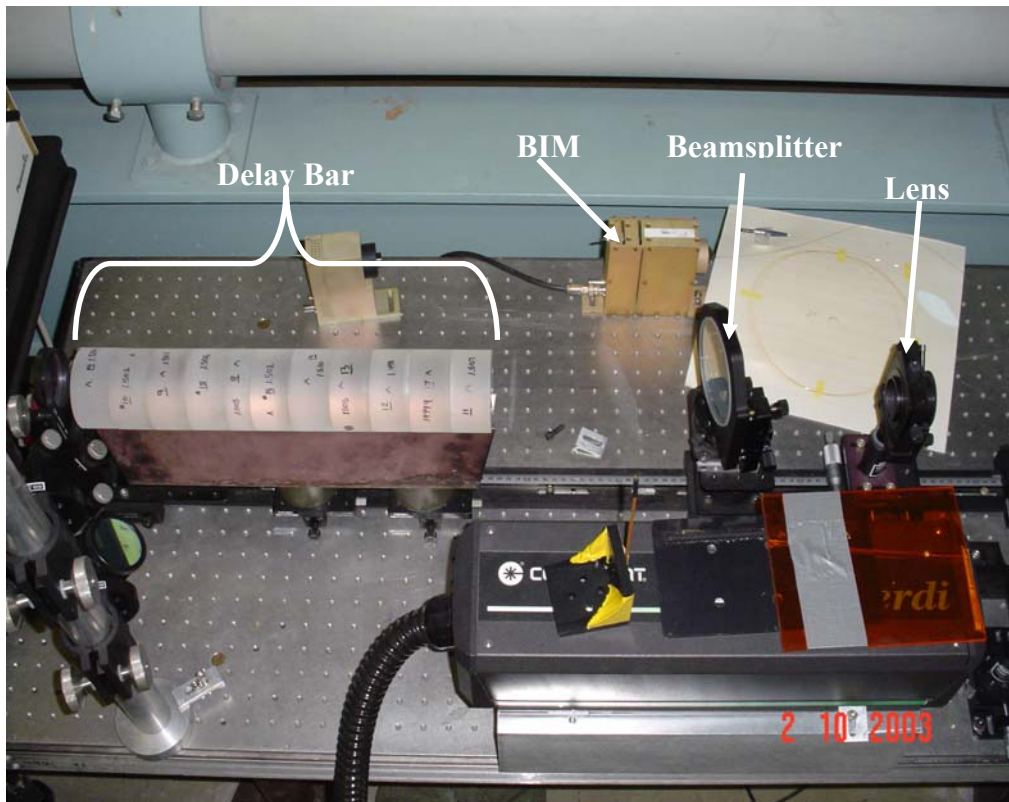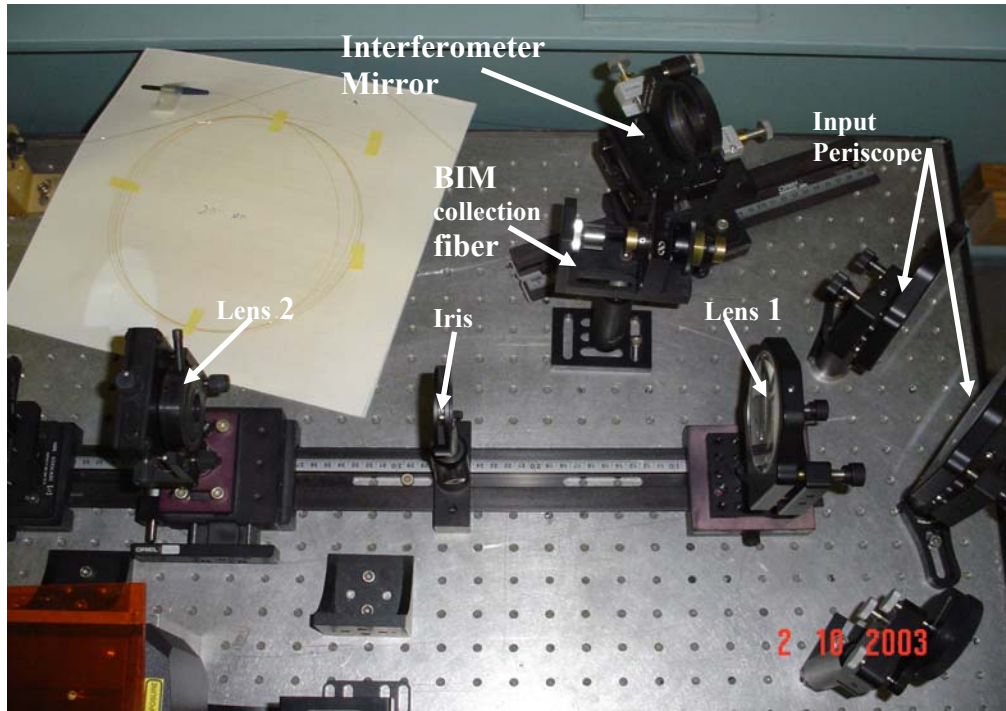
Figure A8. Interferometer Schematic

Figure A9. Details of interferometer proper (Photo)

Each of these beams, because they emerged from the same single source (the laser), carries the same wave profile. In order for the two beams, now split, to interfere with each other creating an interference pattern, they must first be put out of phase from each other. The easiest way to do this is to change the physical path distance one beam must travel prior to re-combining with its split counterpart. In our system, this is done by both moving the M2 mirror back and by adding glass of a known thickness for use as a delay bar. Not only does moving the M2 mirror change the distance of that leg, but it also changes the angle at which the split beam takes to re-combine with the other beam. This slight angular difference is also what helps reveal the interference pattern (see figure A10) caused by the two images at the re-combination plane.
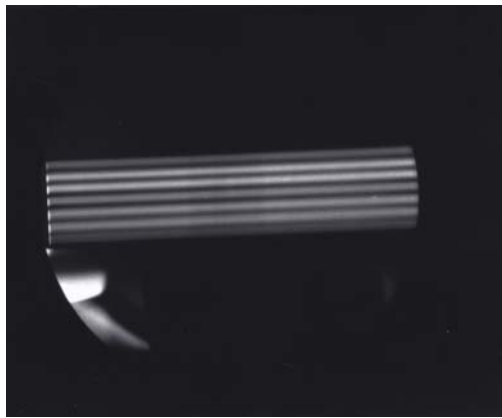

Figure A10. Interference Fringes

Each one of these fringes (light and dark lines) becomes a data point. Across the fringes, is spatial information of the line on the target, and thus the target itself. You are essentially viewing that portion of the target which is being illuminated by your line. Going along the length of the fringes is time. The streak camera creates this time frame when it streaks the image. Any movement or fringe variations during a shot are correlated to the target surface and how it behaved during the impact / shock test.

A.6 Streak Camera / Impulse Dot Generator / Comb Generator

These three items, the streak camera, the impulse dot generator, and the comb generator all work together to provide the user with the following information:

- The streak camera simultaneously measures time, position, and light intensity of the image, and processes the data in real-time.

- The impulse dot generator gives the user an exact time measurement of when an event starts.

- The comb generator provides an output of pulses at a user-defined interval so that a

time base can be established during the streak event. Many impulse dot generators are combined together with the comb generators in one unit.

The streak camera is designed to image what it sees on its slit. It is onto this slit that the re-combined image is projected. The camera basically sees the slit being illuminated by this image in light and dark variations (fringes). The image passes through the slit and is formed by the internal optics into a slit image on the photocathode of the streak tube. The incident light on the photocathode is converted into a number of electrons proportional to the intensity of the light. These electrons then pass through a pair of accelerating electrodes, where high voltage is applied to the electrodes. This voltage is applied at a timing synchronized to the incident light. This initiates a high-speed sweep. The electrons are deflected by the application of high voltage and they are bombarded against a phosphor screen where they are again, converted into light. The amount of light generated by the fluorescent material is proportional to the kinetic energy of the electrons that struck it. This light is usually very faint and only lasts an instant. Because of this, typically, highly sensitive film, or better yet, a high-sensitivity CCD camera is used to capture and record the streak event. This image is then relayed from the CCD for example, through a frame grabber and to a computer where the image can be saved, and eventually, the data can be reduced.

Distribution

Internal:

MS 0323	Dept. 1011	D. L. Chavez (LDRD Office)
MS 0834	Dept. 9112	W. M. Trott
MS 1152	Dept. 1642	M. L. Keifer
MS 1152	Dept. 1643	L. X. Schneider
MS 1153	Dept. 15330-1	M. T. Buttram
MS 1156	Dept. 15322	R. D. M. Tachau
MS 1159	Dept. 15344	M. A. Hedemann
MS 1168	Dept. 1647	L. C. Chhabildas
MS 1168	Dept. 1646	C. A. Hall
MS 1168	Dept. 1646	C. Deeney
MS 1168	Dept. 1647	M. D. Furnish (10)
MS 1168	Dept. 1647	J. Podsednik
MS 1168	Dept. 1647	W. D. Reinhart
MS 1170	Dept. 15310	R. D. Skocypec
MS 1178	Dept. 1630	D. D. Bloomquist
MS 1178	Dpet. 1639	D. L. Kitterman
MS 1178	Dept. 1637	F. W. Long
MS 1179	Dept. 15340	J. R. Lee
MS 1181	Dept. 1610	J-P. Davis
MS 1181	Dept. 1610	R. J. Hickman
MS 1181	Dept. 1610	M. D. Knudson
MS 1181	Dept. 1610	J. Mason
MS 1186	Dept. 1674	T. Mehlhorn
MS 1186	Dept. 1674	R. J. Lawrence
MS 1186	Dept. 1670-1	J. F. Seamen
MS 1190	Dept. 1600	J. P. Quintenz
MS 1191	Dept. 1670	K. Matzen
MS 1192	Dept. 1670-1	T. Gilliland
MS 1192	Dept. 1670-1	C. Russell
MS 1193	Dept. 1673	J. L. Porter
MS 1193	Dept. 1645	J. E. Maenchen
MS 1194	Dept. 1640	D. H. McDaniel
MS 1194	Dept. 1644	K. W. Struve
MS 1196	Dept. 1677	R. J. Leeper
MS 1391	Dept. 1634	D. D. Thomson
MS 9018	Dept. 8945-1	Central Technical Files
MS 0899	Dept. 9616	Technical Library (2)